Catal Lett (2012) 142:42–49
DOI 10.1007/s10562-011-0726-8

Structural, Textural and Acid–Base Properties of Nano-Sized $NiFe_2O_4$ Spinel Catalysts

R. Benrabaa · H. Boukhlouf · S. Barama · E. Bordes-Richard · R. N. Vannier · A. Barama

Received: 4 August 2011 / Accepted: 18 October 2011 / Published online: 5 November 2011

Abstract The effect of preparation methods on the textural, structural and acid–base properties of nano-sized nickel ferrite oxides was investigated. Several physicochemical methods are used for their characterization. Isopropanol, as a probe molecule, is used to determine acid–base properties. A correlation between textural, structural and acid–base properties of nanomaterials is established.

Keywords Co-precipitation · Hydrothermal · Isopropanol · $NiFe_2O_4$

1 Introduction

Spinel ferrite structures have received much attention in the recent years due to their structural, electronic, magnetic and catalytic properties. These materials are good candidates for several applications: in electric and electronic devices, in H_2O, CO_2 and alcohols decomposition, in the oxidation of CO to CO_2 and reforming of CH_4 to syngas [1–3]. $NiFe_2O_4$ is an inverse AB_2O_4 spinel, all Ni^{2+} ions being located in the octahedral B-sites and Fe^{3+} ions equally distributed between tetrahedral A and octahedral B-sites [4]. The catalytic properties of AB_2O_4 spinels strongly depend on the nature of A and B ions, their charge and their distribution among the octahedral Oh and tetrahedral Td sites of the spinel structure. Reithwisch and Dumesic [5] studied a number of spinel structures (normal, mixed and inverse) and concluded that only inverse and mixed spinel structures can readily undergo rapid electron exchange between II + and III + ions.

The catalytic activity and selectivity of metallic oxides, in many oxidation processes, are closely related to their structural, textural and acid–base and/or redox properties [6–10]. Many molecules, such NH_3, CO_2 or isopropanol, were used, as probe reactant, to characterize the surface acid–base properties of these materials. The isopropanol decomposition has been extensively reported as a valuable catalytic test to analyze the surface acid–base properties of heterogeneous catalysts [3, 11]. The decomposition occurs via two parallel elimination pathways: the dehydration to propylene and diisopropyl ether and the dehydrogenation to acetone. The rates and products selectivity for isopropanol decomposition depend on the catalyst surface acid–base properties. Several mechanisms have been proposed in the literature to explain these reactions. It has been postulated that the dehydration elimination reaction proceeds on acidic centers (Brønsted and Lewis acid sites) and the formed propylene rate may be a measure of the acidity of oxides; whereas, the redox (basic) centers are involved in the dehydrogenation path [12]. Gervasini and Auroux

R. Benrabaa · H. Boukhlouf · S. Barama · A. Barama (✉)
Laboratoire de Matériaux Catalytiques & Catalyse en Chimie Organique, Faculté de Chimie, USTHB, BP32 El Alia, 16111 Bab Ezzouar, Alger, Algérie
e-mail: a_barama@yahoo.fr

R. Benrabaa
e-mail: rafikemp@gmail.com

H. Boukhlouf
e-mail: boukhloufhamza@gmail.com

S. Barama
e-mail: siham_barama@yahoo.com

E. Bordes-Richard · R. N. Vannier
Unité de Catalyse et de Chimie du Solide, UMR CNRS 8181, Université des Sciences et Technologies de Lille, Cité scientifique, 59655 Villeneuve d'Ascq, France
e-mail: Elisabeth.Bordes@univ-lille1.fr

R. N. Vannier
e-mail: Rose-Noelle.vannier@ensc-lille.fr

[13] attempted to correlate the dehydration and dehydrogenation activities of isopropanol decomposition with the acid–base character obtained by the calorimetric investigation [14] of a large series of metal oxides. The isopropanol decomposition cannot distinguish between the Brønsted and Lewis acidity. Nevertheless, Aramendia et al. [15] have reported that the dehydration activity during isopropanol decomposition could be correlated with Brønsted acidity.

In the present work, $NiFe_2O_4$ oxides were synthesized by co-precipitation (CP) and hydrothermal (HT) methods, characterized by different techniques and tested in isopropanol decomposition reaction. The purpose is to evaluate the effect of preparation method and calcination temperature on the structural, textural and acid–base properties of nanomaterials spinel $NiFe_2O_4$.

2 Experimental

2.1 Catalysts Preparation

The materials were synthesized by CP and HT methods and synthesis protocol is described in detail previously in [16]. The samples prepared by CP method and annealed at various temperatures (650, 750 and 850 °C) for 4 h are noted CP-650, CP-750 and CP-850. The solid obtained by HT process and treated at 140 °C for 12 h is noted HT-140.

2.2 Characterization

All samples were characterized using the following physicochemical methods: X-ray powder diffraction (XRD) was performed on a Bruker AXS D8 Advance diffractometer working in Bragg–Brentano geometry using Cu Kα radiation ($\lambda = 1.54$ Å), equipped with an energy dispersive detector (Sol-X). Patterns were collected at room temperature, in the $2\theta = 10$–$90°$ range, with a 0.02° step and 10 s counting time per step. The EVA software attached to the Bruker machine was used for phase identification and unit-cell parameters and crystallite size (C_s) were refined by *Rietveld* method using the Fullprof program and its winplotr interface [17]. X-ray diffraction at variable temperatures (HT-XRD) under air atmosphere was carried out on the same apparatus equipped with XRK 900 chamber and a Vantec detector up to 800 °C. Diagrams were collected every 25 °C at 0.1 °C/s heating rate, the counting time being chosen to collect a diagram in 15 min in the 10–90° 2θ range. The sample was displayed on a platinum sheet and air was flowed in the chamber (5 L/h). TG-DTA was performed on a SETARAM TG-92 in combination with analysis of released gases by mass spectrometry (Pfeiffer). Ca. 20 mg of sample was heated at 5 °C/min in air flow from 25 to 1000 °C. Laser Raman Spectroscopy (LRS) was performed with a Spectra Physics krypton ion laser at room temperature with the 647.1 nm excitation line. The beam was focused onto the samples using the macroscopic configuration of the apparatus. To avoid their damage due to absorption, all compounds were studied with a very low laser power (3 mW on the sample). Four accumulations were used in each spectral range. No damage of the material by the laser was observed. The scattered light was analyzed with an XY Raman Dilor spectrometer equipped with an optical multichannel charge coupled device liquid nitrogen-cooled detector. The spectral resolution was approximately 0.5 cm^{-1} in the 200–1500 cm^{-1} range. Acquisition and data processing were performed with the LABSPEC software. Fourier Transformed Infra Red spectroscopy (FTIR) spectra were obtained at a resolution 2 cm^{-1} and 60 scans, between 4000 and 400 cm^{-1}, using a model Schumadzu 8400S on samples pelletized with KBr powder (3% of powder was mixed with 97% of KBr). The specific surface area (S_{BET}) of the samples was determined by nitrogen adsorption at −196 °C with a Micromeritics ASAP2010 apparatus. Scanning electron microscopy (SEM) and X-ray energy dispersive microanalysis (EDX) were carried out on a HITACHI 4100S apparatus at 6 kV. Solids were ground as fine particles and mechanically dispersed on an electrically conductive carbon tape which was placed on an aluminum disc. X-ray photoelectron spectroscopy (XPS) was carried out on an Escalab 220 XL spectrometer (Vacuum Generators). A monochromatic Al Kα X-ray source was used and electron energies were measured in the constant analyzer energy mode. The pass energy was 100 eV for the survey of spectra and 40 eV for the single element spectra. All XPS binding energies were referred to C1s core level at 285 eV. The angle between the incident X-rays and the analyzer was 58°, photoelectrons being collected perpendicularly to the sample surface. Spectra were analyzed with the CasaXPS software. The catalytic tests in isopropanol decomposition were carried out between 200 and 500 °C in a fixed bed continuous flow reactor under atmospheric pressure and in the absence of oxygen, by passing the carrier gas (Nitrogen) through a saturator containing the alcohol and maintained at 273 K. The weight of catalyst was ca. 0.05 g and the flow rate was 40 mL STP min^{-1}. Product analysis was performed by gas chromatography using a 10% Carbowax 20 M on Chromosorb 200 column and a Flame ionisation detector.

The conversion of isopropanol (C %), selectivity of propene (Spr %) and selectivity of acetone (Sac %) were calculated using the following equations:

$$C(\%) = \frac{\text{Moles of isopropanol converted}}{\text{Moles of isopropanol in feed}} \times 100 \qquad (1)$$

$$\mathrm{Spr}(\%) = \frac{\text{Moles of propylene produced}}{\text{Moles of isopropanol converted}} \times 100 \quad (2)$$

$$\mathrm{Sac}(\%) = \frac{\text{Moles of acetone produced}}{\text{Moles of isopropanol converted}} \times 100 \quad (3)$$

3 Results and Discussion

3.1 Thermal Analysis of CP Precursor and HT Catalyst

The decomposition in air of CP-80 precursor and of HT-140 catalyst was studied by TG-DTA-MS in the 25–1000 °C range (Fig. 1). The successive weight losses (%), the corresponding temperatures and the nature of evolved gases are gathered in Table 1. After loss of adsorbed water, three steps were observed during the decomposition of CP-80 up to 660 °C (Fig. 1a). The presence of CO_2 during the first step let suppose that some carbonates were decomposing. During the following steps the release of NO_x was observed twice for CP-80 (Table 1). The theoretical weight loss for the transformation of $Ni(OH)_2 + 2\,Fe(OH)_3$ to $NiFe_2O_4$ is $\Delta m/m = 33.7\%$. This value was approximately reached (35.0%) in

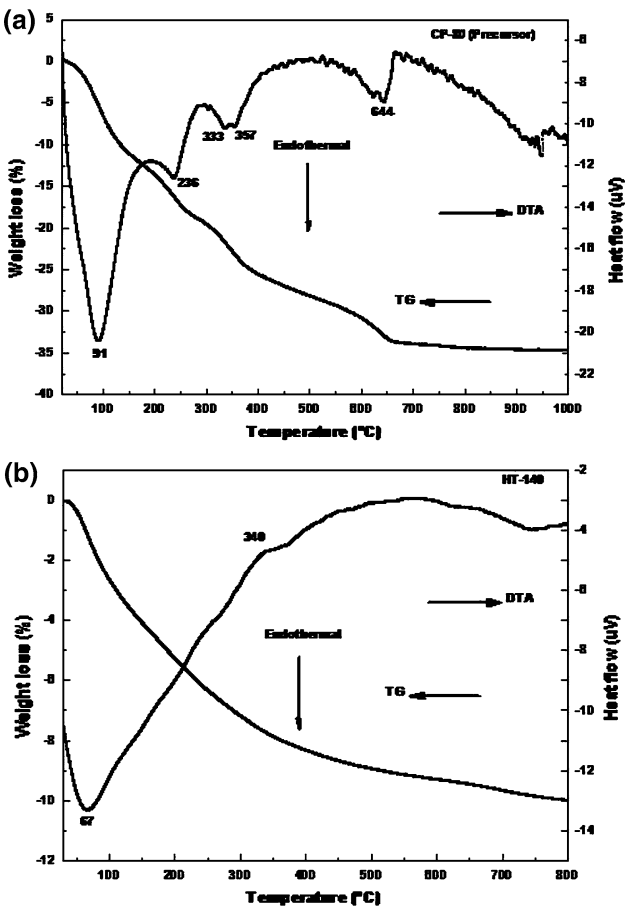

Fig. 1 TG-DTA curves in air of CP-80 precursor (**a**) and HT-140 catalyst (**b**)

Table 1 TG-DTA-MS of CP-80 and HT-140 heated in air

Sample	Temperature[a] (°C)	Released gas	Temperature[b] (°C)	Δm/m[b] (%)
CP-80	126	H_2O	125	11.5
	260	H_2O, CO_2	270	19.5
	380	NO, NO_2	385	26.7
	660	NO	660	35.0
HT-140	158	H_2O	100	3.5
	313	CO_2	290	10.0

[a] DTA-MS signals

[b] Successive weight losses; Change of slope of weight versus temperature curve

the case of CP-80 precursor. In comparison, for HT-140, the continuous weight loss (about 10%) (Fig. 1b) could be assigned to the decomposition of some remaining hydroxides and carbonates. The transformation of CP precursor was studied by HT-XRD up to 800 °C in air (Fig. 2). The precursor of CP was amorphous up to 500 °C, temperature at which the lines of $NiFe_2O_4$ started to grow. At 800 °C the spinel was the main compound observed, but additional peaks were observed in the 30–35° range. Moreover, another peak was observed at $2\theta = 29.3°$, which disappeared above 400 °C. These lines account for the formation of $NaHCO_3$ that may have formed in solution (pKa = 10.6 for HCO_3^-/CO_3^{2-}), as due to the presence of some carbonates in NaOH. This finding was in accordance with the high amount of CO_2 observed during TG-DTA-MS of CP-80. Taking into account these results, it was decided to calcine CP-80 solid at 650, 750 and 850 °C.

3.2 Structural Properties Characterization of CP and HT Catalysts

XRD data of the CP and HT-samples are shown in Fig. 3. They indicated that the precursor is nearly amorphous. On the other hand, for all CP and HT-samples, XRD patterns are consistent with the well-crystallized solids. $NiFe_2O_4$ crystalline phase is observed for all CP and HT systems. For HT-sample, the spectrum showed only the lines characteristic of pure $NiFe_2O_4$ (PDF 00-054-0954) structure. While, for the CP catalysts, annealed at various temperatures in the range 650–850 °C, XRD analysis showed, besides the lines of $NiFe_2O_4$, the presence of characteristic signals of Na_2CO_3 (PDF 00-008-0448) and likely traces of other oxides. No diffraction peaks of Fe_2O_3 or NiO free oxides were observed for all preparations. The crystallite size (C_s) was refined by *Rietveld* method. A crystallite size of 23 nm was derived for the spinel in CP-650, it increased to 56 nm and 77 nm after annealing at 750 and 850 °C, respectively (Table 2). The unit-cell parameter undergoes a slight decrease when the temperature of annealing

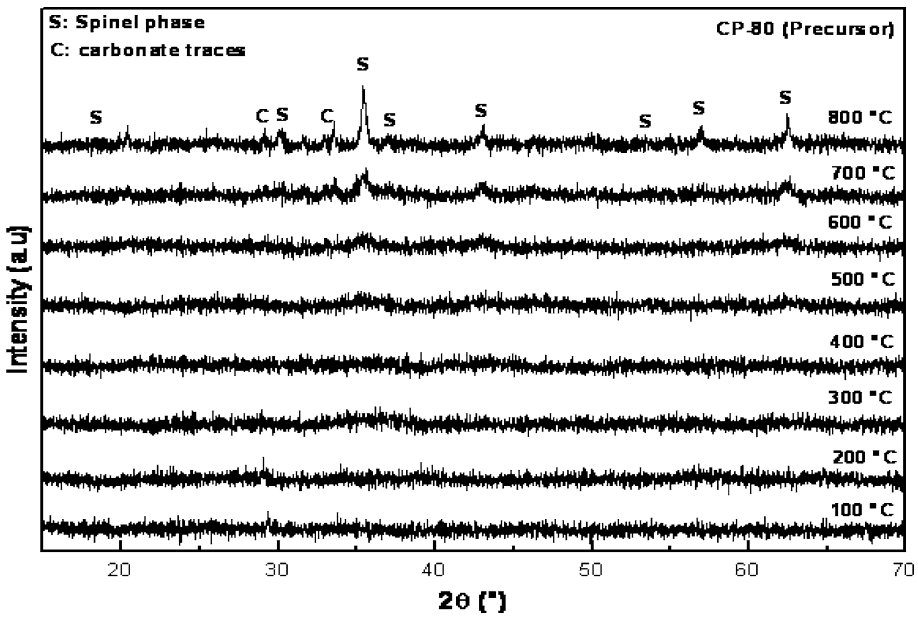

Fig. 2 XRD patterns at high temperatures of CP-80 precursor

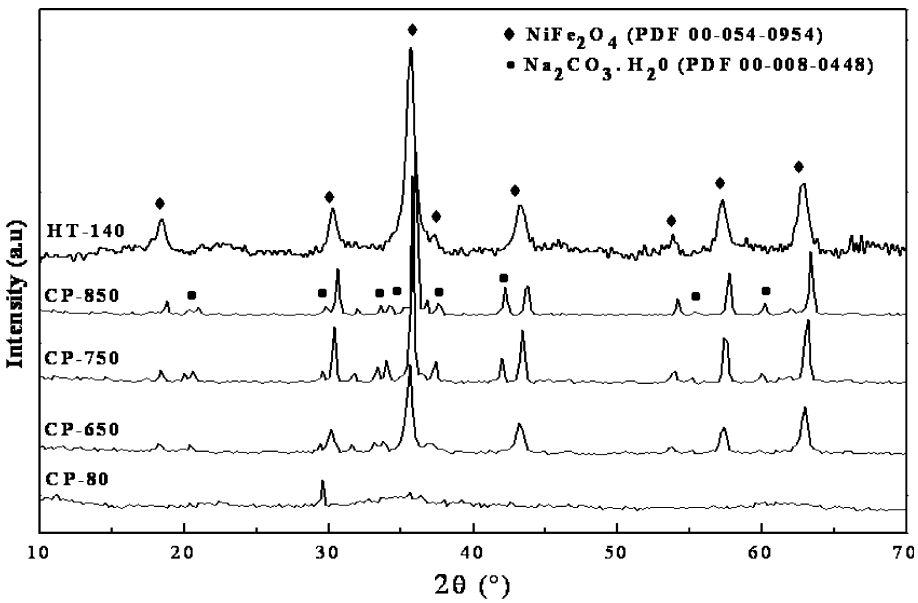

Fig. 3 XRD patterns of $NiFe_2O_4$ samples prepared by CP and HT methods

Table 2 Textural and surface properties of CP and HT nanomaterials

Catalyst	B.E.T.	XRD[a]		EDS[b]	XPS data[c]			
	S_{BET} (m^2/g)	C_s[a] (nm)	A[a] (Å)	Fe/Ni	Fe[c]	Ni[c]	Na[c]	Fe/Ni
CP-650	2	23	8.341 (8)	2.1	710.5	854.3	1071.8	4.8
CP-750	3	56	8.341 (8)	2.5	710.1	854.1	1071.4	3.7
CP-850	2	77	8.337 (7)	2.1	710.7	855.2	1071.8	5.0
HT-140	37	9	8.360 (2)	1.9	710.7	854.9	–	1.8

[a] Calculated using Rietveld refinement

[b] Theoretical atomic ratio Fe/Ni = 2

[c] Binding energy (eV)

increases. According to XRD data, the incorporation of iron and nickel in the $NiFe_2O_4$ structure is not complete at 850 °C for the CP catalysts. These results are in agreement with those of M. M. Rashad et al. [18] who showed that the formation of pure phase $NiFe_2O_4$, using co-precipitation method, is observed around 1200 °C.

Raman spectra (Fig. 4) are in agreement with XRD results. They revealed, for CP and HT materials, the presence of Raman bands at ca. 333, 381, 449, 488, 571, 592, 661 and 703 cm^{-1} that have been assigned to the presence of inverse $NiFe_2O_4$ phase [19, 20]. The strong band at 703 cm^{-1} is a common feature of the Raman spectra of the inverse spinel [20, 21]. For the CP compounds, the band, observed at 1080 cm^{-1}, is attributed, in agreement with our XRD analysis, to the carbonate species. The Raman spectrum of pure sample describes the same features that those found in the literature [21–23].

IR spectra (Fig. 5) showed, for CP and HT ferrites spinel, two principal absorption bands around 600 and 400 cm^{-1} assigned to the vibration of metallic ions in the crystal lattice [24]. In the case of CP-solids, the intensity of these bands increases with increasing the heat-treatment temperature, this is probably due to the increase of size of the $NiFe_2O_4$ nanocrystals. It is known that in the spinel structure, the metallic ions are distributed among the tetrahedral (Td metal–oxygen) and octahedral (Oh metal–oxygen) spinel sites. The highest frequency band at ca. 600 cm^{-1} is assigned to the vibration of the Td metal–oxygen group and the band at ca. 400 cm^{-1} are associated to the vibration of the Oh metal–oxygen group [25]. The difference, in the absorption position in octahedral and tetrahedral complexes of $NiFe_2O_4$ crystal, is due to the difference in distance between Fe^{3+} and O^{2-} in the octahedral and tetrahedral sites.

3.3 Textural and Surface Properties

The stoichiometry of all prepared solids was verified using X-ray energy dispersive microanalysis (EDX). The obtained results are reported in Table 2. The measured Fe/Ni atomic ratio of all analyzed samples, are very similar to the nominal atomic ratios used in the preparations, excepted for CP-750 (Fe/Ni = 2.5). For all CP-solids, EDX analysis confirms the traces of Na species observed by XRD and Raman analysis. The SEM micrographs (Fig. 6), of CP-650 and HT-140 catalysts, revealed clearly, for the CP sample, a heterogeneous system with grains of different size and for HT-sample, a system relatively homogeneous with smaller grains.

The specific surface area S_{BET} (table 2), for all CP samples, is very low (<4 m^2/g) compared to the HT-sample (37m^2/g). This difference is in agreement with the crystallites size (C_s) calculated using XRD data (23-77 nm for CP-solids against 9 nm for HT solid). The low specific surface area, observed for the CP samples, is due probably to the presence of sodium species which clogs the pores and also to the high temperatures of solid pretreatment (650–850 °C) which favor the particles sintering.

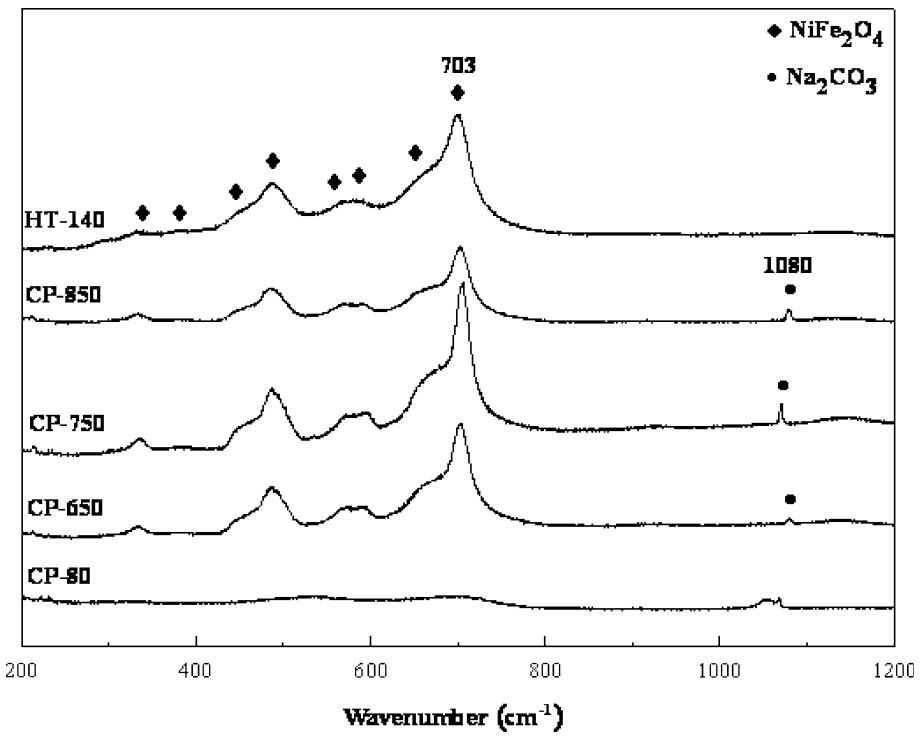

Fig. 4 Raman spectra in 200–1200 cm^{-1} range of CP and HT samples

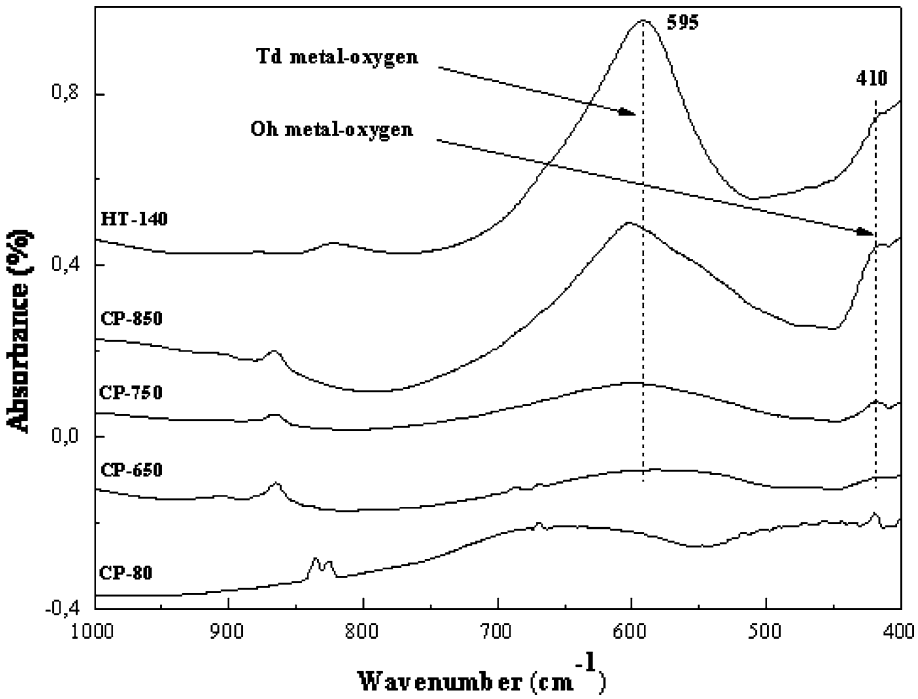

Fig. 5 FTIR spectra in 1300–400 cm^{-1} range of CP and HT materials

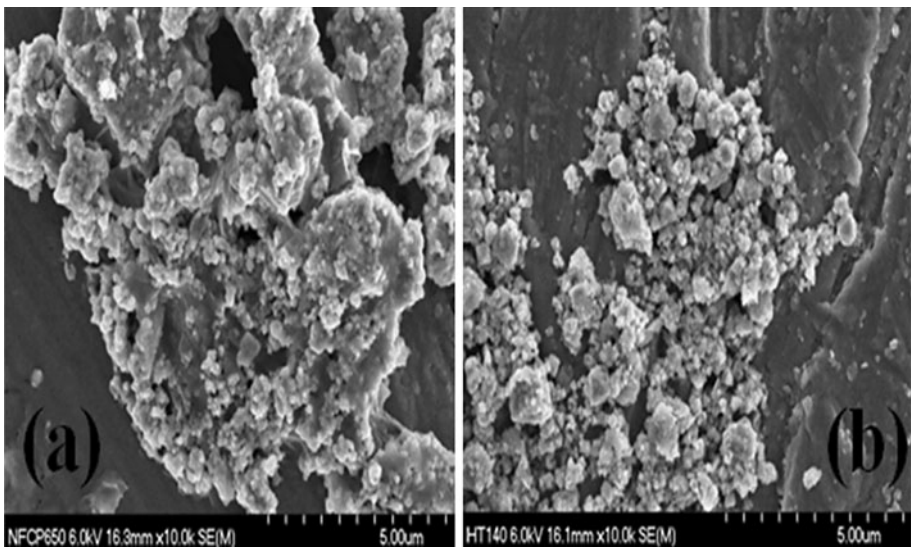

Fig. 6 Scanning electron micrographs of CP-650 (**a**) and HT-140 (**b**) samples

XPS analyses were performed in order to determine the surface composition of the materials and the oxidation states of Ni and Fe. Ni(II) and Fe(III) were detected in all catalysts by the Ni $2p_{3/2}$ and Fe $2p_{3/2}$ photopeaks. The binding energies (BE) of Ni$2p_{3/2}$ and Fe$2p_{3/2}$ photopeaks for CP and HT-samples are reported in Table 2. The values of the binding energies for Ni$2p_{3/2}$ (854.1–855.2 eV) and Fe$2p_{3/2}$ (710.1–710.7 eV) were typical of Ni^{2+} and Fe^{3+} species [26–29]. The presence of sodium on the CP-solids surface was detected by the binding energies at 1071.4–1071.8 eV. Generally, the photopeak position depends on the preparation method and on the temperature of pretreatment. The differences, observed between the binding energies, are probably due to the difference of the chemical environment of the species. Important difference in Ni and Fe surface concentration are observed between CP and HT solids. For the CP-solids, the values of surface Fe/Ni ratio are very high as compared to the theoretical values used during preparation, meaning that most of iron is present on the solid surface. On the other hand, for HT-sample, the Fe/Ni ratio is very close to the expected values, indicating a good dispersion of nickel on the HT-140 surface. The calcination

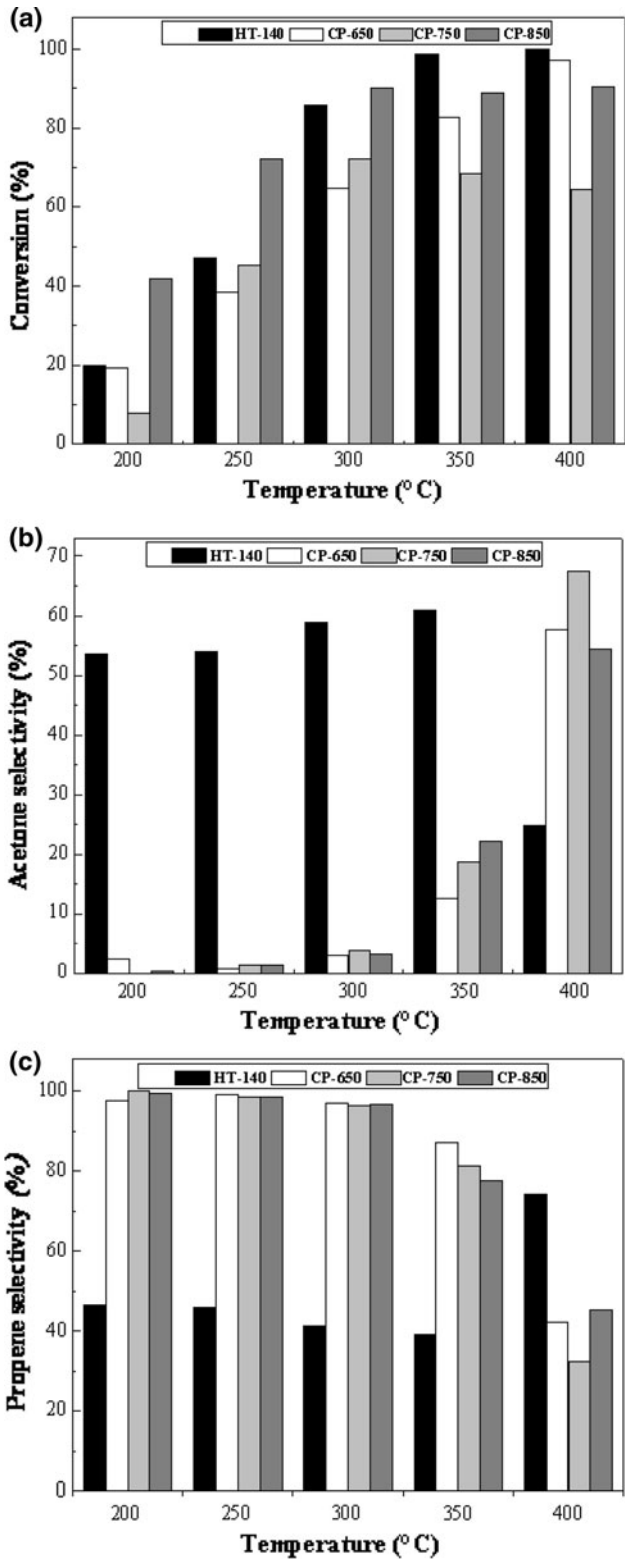

Fig. 7 Isopropanol conversion (**a**), acetone selectivity (**b**) and propylene selectivity (**c**)

temperature does not seem to have a significant influence on the surface composition as indicated by the Fe/Ni ratios of CP-650 (4.8), CP-750 (3.7) and CP-850 (5).

3.4 Isopropanol Decomposition

The conversion of isopropanol and the selectivity to propylene and acetone, obtained on nickel ferrite oxides, are presented in Fig. 7. In all cases, propylene and acetone were detected but no diisopropyl ether (condensation products) was observed; propylene is due to the presence of acid sites, and acetone to that of basic sites. The isopropanol conversion (Fig. 7a) increased with the reaction temperature on all samples. This increase is faster on HT-140 catalyst in accordance with its higher surface area (37 m^2/g against 2–3 m^2/g for CP-solids), a smaller crystallite size, a lower temperature reduction and a higher dispersion of nickel active species as shown by the difference between the atomic Fe/Ni ratios determined by XPS and EDS for HT and CP samples. The product distribution of isopropanol decomposition depended strongly on the catalyst surface composition. The selectivity towards dehydrogenation and dehydration reactions was much affected by changing the reaction temperature and preparation method. For HT-140, acetone and propylene were observed throughout the temperatures range 200–400 °C, which means that both acidic and basic sites were available (Fe/Ni = 1.9). At 350 °C, the selectivity to acetone was 61%, but decreased and became null at 450 °C (Fig. 7b). In contrast, on CP systems, the dominating species were mostly "acidic" at low temperature. Upon increasing temperature, the selectivity to propylene decreased from ~82% at 350 °C to ~40% at 400 °C (Fig. 7c), while the sites responsible for dehydrogenation increased. This decrease (for CP-solids) and increase (for HT-sample) of propylene selectivity could be directly related to the reducibility of metallic species observed by H_2-TPR [16] and to the surface structure, performed by XPS analysis. Changes in acid–base properties of HT, when the reaction temperature increases (from 350 to 400 °C), could be due to the migration, towards the surface, of Fe^{3+} species which is most acidic compared to Ni^{2+} [30]. The high acidity of CP samples, confirmed by propylene production, is certainly due to the high surface concentration of Fe^{3+} ions, observed by XPS analysis. The temperature of calcination of this category (CP samples) did not influence markedly the product distribution which is almost similar for all solids.

4 Conclusion

Nanocrystalline $NiFe_2O_4$ powders have been successfully synthesized by CP and HT methods. The HT method presented many advantages compared to the CP method. It led to the formation of a pure crystalline nickel ferrite $NiFe_2O_4$ at low temperature, while a mixed phase has been formed

by CP technique in the temperature range 650–850 °C. In addition, the HT-sample presented the better specific surface area of 37 m^2/g (against 2–3 m^2/g for CP-solids). A great difference in the surface composition of HT and CP-solids was observed (XPS analysis). The best nickel dispersion is achieved on HT-sample. The isopropanol decomposition was used to determine the acid–base properties of the catalysts. Propylene and acetone were detected. The product distribution depends mainly on the catalyst composition. Isopropanol dehydration to propylene, which is an indication of acid character, predominate on CP samples up to 350 °C; while, the dehydrogenation and dehydration reactions to acetone and propylene, respectively, related to the contribution of both acidic and basic sites, is favored on HT-sample.

Acknowledgment Authors send their heartfelt thanks to N. Djellal, L. Burylo, A-S. Mamède, M. Frère and A. Laubrin for their ideas and fruitful discussions.

References

1. Baruwati B, Reddy K, Manorama S, Singh R, Parkash Om (2004) Appl Phys Lett 85:2833
2. Miroslaw MB, Krzysztof H (2007) J Eur Ceram Soc 27:723
3. Bocanegra SA, Ballarini AD, Scelza OA, De Miguel SR (2008) Mater Chem Phys 111:534
4. Wells AF (1984) Structural Inorganic Chemistry. Clarendon Press, Oxford
5. Reithwisch DG, Dumesic (1986) J A Appl Catal 21:97
6. Xiaoyan T, Guiying L, Ying Z, Changwei Hu (2010) J Alloy Compd 493:55
7. Pozo Lopez G, Silvetti SP, Aguirre M, Condo AM (2009) J Alloy Compd 487:646
8. Kavas H, Kasapoglu N, Baykal A, Köseoglu Y (2009) Chem Pap 63(4):450
9. Mathew T, Tope BB, Shiju NR, Hegde SG, Rao BS, Gopinath CS (2002) Phys Chem Chem Phys 4:4260
10. Lázár K, Mathew T, Koppány Z, Megyeri J, Samuel V, Mirajkar SP, Rao BS, Guczi L (2002) Phys Chem Chem Phys 4:3530
11. Wang JA, Bokhimi X, Novaro O, Lopez T, Gomez R (1999) J Mol Catal A 145:291
12. Trikalitis PN, Pomonis PJ (1995) Appl Catal A 131:309
13. Gervasini A, Auroux A (1991) J Catal 131:190
14. Auroux A, Gervasini A (1990) J Phys Chem 94:6371
15. Aramendia MA, Borau V, Jimenez C, Marinas JM, Porras A, Urbano FG (1996) J Catal 161:829
16. Benrabaa R, Boukhlouf H, Bordes-Richard E, Vannier RN, Barama A (2010) Stud Surf Sci Catal 175:301
17. Rodríguez-Carvajal J (2001) Recent developments of the program FULLPROF, in commission on powder diffraction (IUCr) Newsletter 26:12
18. Rashad MM, Fouad OA (2005) Mater Chem Phy 94:365
19. Shi Y, Ding J, Shen ZX, Sun WX, Wang L (2000) Solid State Comm 115:237
20. Ivanov VG, Abrashev MV, Iliev MN, Gospodinov MM, Meen J, Aroyo MI (2010) Phys Rev B82 024104:1
21. De Paiva JAC, Graca MPF, Monteiro J, Macedo MA, Valente MA (2009) J Alloy Compd 485:637
22. Kreisel J, Lucazeau G, Vincent H (1998) J Solid State Chem 137:127
23. Hannoyer B, Ristic M, Popovic S, Music S, Petit F, Foulon B, Dalipi S (1998) Mater Chem Phys 55:215
24. Gunjakar JL, More AM, Shinde VR, Lokhande CD (2008) J Alloy Compd 465:468
25. Liu Y-L, Wang H, Yang Y, Liu Z-M, Yang H-F, Shen G-L, Yu R-Q (2004) Sens Actuators B 102:148
26. Mathew T, Shylesh S, Devassy B, Vijayaraj M, Satyanarayana C, Bollapragada S, Rao BS, Gopinath CS (2004) Appl Catal A 273:35
27. Florea MA, Parvulescu VI, Mihaila-Tarabasanu D, Diamandescu L, Feder M, Negrila C, Frunza L (2009) Catal Today 141:361
28. Vijayaraj M, Chinnakonda S (2006) J Catal 241:83
29. Mathew T, Shiju NR, Bokade VV, Rao BS, Gopinath CS (2004) Catal Lett 94:223
30. Ramankutty CG, Sugunan S, Thomas B (2002) J Mol Catal A 187:105